

# Chapter 2

## Subcriticality



Kengo Hashimoto

**Abstract** For a subcritical reactor system driven by a periodically pulsed spallation neutron source in KUCA, the Feynman- $\alpha$  and the Rossi- $\alpha$  neutron correlation analyses are conducted to determine the prompt neutron decay constant and quantitatively to confirm a non-Poisson character of the neutron source. The decay constant determined from the present Feynman- $\alpha$  analysis well agrees with that from a previous analysis for the same subcritical system driven by an inherent source. Considering the effect of a higher mode excited, the disagreement can be successfully resolved. The power spectral analysis on frequency domain is also carried out. Not only the cross-power but also the auto-power spectral density have a considerable correlated component even at a deeply subcritical state, where no correlated component could be previously observed under a 14 MeV neutron source. The indicator of the non-Poisson character of the present spallation source can be obtained from the spectral analysis and is consistent with that from the Rossi- $\alpha$  analysis. An experimental technique based on an accelerator-beam trip or restart operation is proposed to determine the subcritical reactivity of ADS. Applying the least-squares inverse kinetics method to the data analysis, the subcriticality can be inferred from time-sequence neutron count data after these operations.

**Keywords** Subcriticality · Prompt neutron decay constant · Feynman- $\alpha$  method · Rossi- $\alpha$  method · Power spectral analyses

---

K. Hashimoto (✉)

Atomic Energy Research Institute, Kindai University, Osaka, Japan

e-mail: [kengoh@pp.ij4u.or.jp](mailto:kengoh@pp.ij4u.or.jp)

© The Author(s) 2021

C. H. Pyeon (ed.), *Accelerator-Driven System at Kyoto University Critical Assembly*,  
[https://doi.org/10.1007/978-981-16-0344-0\\_2](https://doi.org/10.1007/978-981-16-0344-0_2)

## 2.1 Feynman- $\alpha$ and Rossi- $\alpha$ Analyses

### 2.1.1 Experimental Settings

#### 2.1.1.1 Core Configurations

The Feynman- $\alpha$  and the Rossi- $\alpha$  neutron correlation analyses considering a non-Poisson character of the spallation source [1] are carried out in the A-core that has two kinds of fuel assemblies: 1/8" P60EUEU and 1/8" P4EUEU. Figure 2.1 shows a side view of the fuel assembly referred to as 1/8" P60EUEU. Fuel and moderator plates of the assembly were set in a 1.5 mm-thick aluminum sheath and the cross section of these plates within the assembly was the square of 2" (50.8 mm). The fuel assembly consisted of 60 unit cells. The unit cell was composed of two (1/16" thick) uranium plates with Al cladding and one (1/8" thick) polyethylene plate. Each of the fuel assemblies had 120 sheets of the uranium plates. The active height of the core, namely 60 unit cells, was 15" (about 38 cm). Adjacent to both axial sides of the active region of each fuel assembly, about 22" (57 cm) upper and 24" (52 cm) lower polyethylene reflectors were attached, respectively. Another fuel assembly referred to as 1/8" P4EUEU consisted of 4 unit cells with upper and lower polyethylene reflectors. The core configuration employed in this study is shown in Fig. 2.2. The twenty-five 1/8" P60EUEU assemblies and one 1/8" P4EUEU assembly were loaded on a grid plate to constitute a critical reactor core. The core was surrounded with many polyethylene-reflector assemblies.

The subcriticality for the present experiment was adjusted by changing the axial position of the central fuel loading [3], as well as the positions of safety and control rods. These subcritical and critical patterns employed in the present experiments are shown in Table 2.1, where these respective subcriticalities are calculated by the continuous-energy Monte Carlo code MVP version 3 (MVP3) [3, 4] with the nuclear data library JENDL-4.0 [5] are also included. The error of the subcriticality indicates statistical uncertainty  $\pm 1\sigma$  of the MVP calculation.

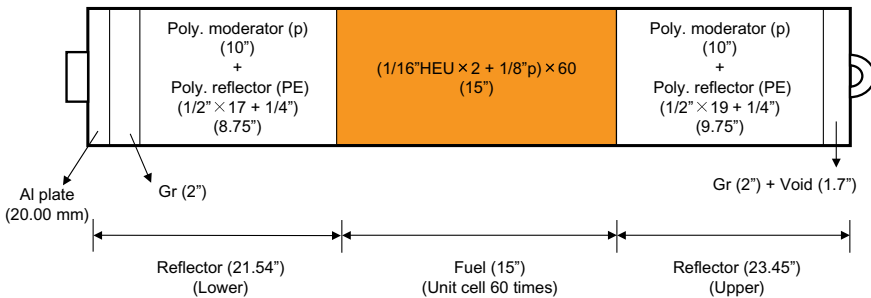


Fig. 2.1 Description of 1/8" P60EUEU fuel assembly (Ref. [2])

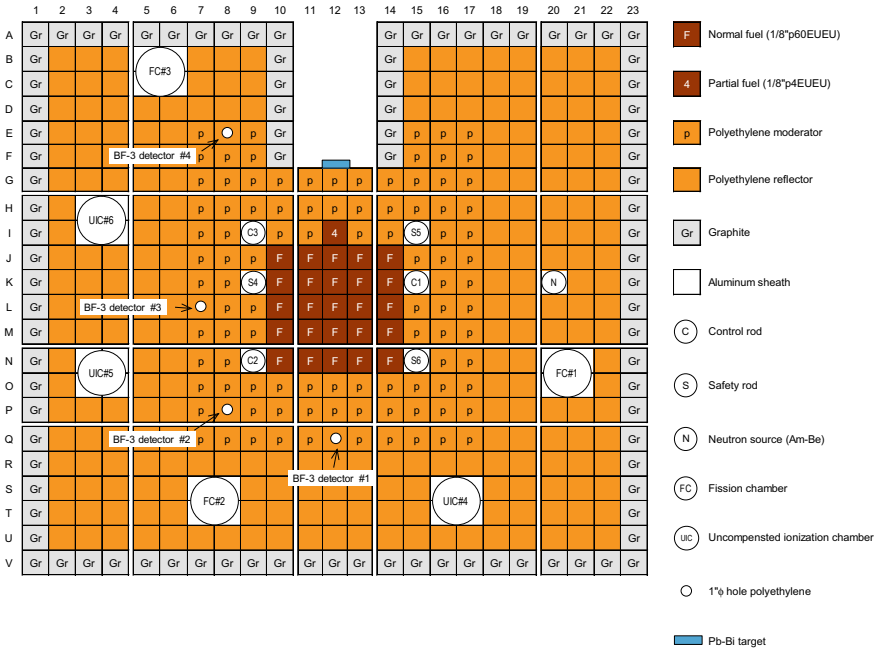


Fig. 2.2 Top view of core configuration and neutron detector location (Ref. [1])

Table 2.1 Experimental patterns of control rods and central fuel loading (Ref. [1])

Subcritical Pattern	Axial position [mm]						Central Loading	Subcriticality [%Δk/k]
	C1	C2	C3	S4	S5	S6		
Critical	U.L.	678.98	U.L.	U.L.	U.L.	U.L.	C.I.	
A	U.L.	L.L.	U.L.	U.L.	U.L.	U.L.	C.I.	0.307 ± 0.008
B	L.L.	U.L.	U.L.	U.L.	U.L.	U.L.	C.I.	0.725 ± 0.018
C	L.L.	L.L.	L.L.	U.L.	U.L.	U.L.	C.I.	1.483 ± 0.040
D	L.L.	L.L.	L.L.	U.L.	U.L.	L.L.	C.I.	2.056 ± 0.054
E	L.L.	L.L.	L.L.	L.L.	L.L.	L.L.	C.I.	3.189 ± 0.083
F	L.L.	L.L.	L.L.	L.L.	L.L.	L.L.	C.W.	13.604 ± 0.381

L.L.: Lower Limit [0 mm], U.L.: Upper Limit [1200 mm]  
 C.I.: Completely Inserted, C.W.: Completely Withdrawn

### 2.1.1.2 Experimental Conditions

Four BF<sub>3</sub> proportional neutron counters (LND-202101, 1” dia., 15.47” len.) were used for the present experiment. These BF<sub>3</sub> counters on locations (Q, 12), (P, 8), (L, 7), and (E, 8) are referred to as B1, B2, B3, and B4, respectively. The axial center of effective length of these counters was located at the axial center position

of active region of the fuel assembly. The present nuclear instrumentation system consisted of conventional detector bias-supply, pre-amplifier, spectroscopy amplifier, and discriminator modules. Finally, signal pulses from these  $\text{BF}_3$  neutron counters were fed to a time-sequence data acquisition system, which registered the arriving time of the signal as digital data. The time length of the acquired data for each subcritical pattern was about 30 min.

The pulsed proton beams were supplied by a fixed-field alternating gradient (FFAG) accelerator. The proton beam intensity of the accelerator was set to 30 pA for any subcritical patterns except for pattern A. For only pattern A, we necessarily made the proton beam intensity fall to 12 pA, to reduce counting loss originated from the dead-time effect of neutron counter. Throughout the present accelerator operations, the pulsed repetition frequency and the beam width were set to 30 Hz and 100 ns, respectively.

## 2.1.2 Formulae for Data Analyses

### 2.1.2.1 Feynman- $\alpha$ Formula

Rana and Degweker [6] derived the Feynman- $\alpha$  and the Rossi- $\alpha$  formulae for a periodically pulsed non-Poisson source, where delayed neutron contribution was considered and each pulse was assumed to be a delta function. Since the pulse width of 100 ns of our accelerator is much shorter than the time scale of the present correlation analyses, the assumption is acceptable. First, we consider the zero-power transfer function  $G(s)$  as follows:

$$\frac{1}{G(s)} = s \left( \Lambda + \sum_{i=1}^7 \frac{\beta_i}{\lambda_i + s} \right) - \rho, \quad (2.1)$$

where the six group model of delayed neutrons is supposed. When the poles and the residues of the above transfer function are represented by  $s_i$  and  $A_i$ , respectively, a parameter  $Y_i$  of the Feynman- $\alpha$  analysis can be defined as [7].

$$Y_i = 2 \frac{\overline{\nu(\nu - 1)}}{\bar{\nu}^2} \frac{A_i G(\alpha_i)}{\alpha_i}, \quad (2.2)$$

where

$$\alpha_i = -s_i. \quad (2.3)$$

Then, the Feynman- $\alpha$  formula derived by Rana and Degweker [6] can be written as follows:

$$\begin{aligned}
Y(T) = & \frac{\bar{v}^2 \lambda_d}{m_1} \sum_{i=1}^7 Y_i \left( 1 - \frac{1 - e^{-\alpha_i T}}{\alpha_i T} \right) \left\{ m_1 \lambda_f + \frac{(m_2 - m_1^2)(-\rho)}{v(v-1)\Lambda} \right\} \\
& + \frac{\bar{v}^2 \lambda_d m_1 (-\rho)}{v(v-1)\Lambda} \sum_{i=1}^7 Y_i \left\{ \frac{e^{-\alpha_i \left(T - \frac{[fT]}{f}\right)} + e^{-\frac{\alpha_i}{f}} e^{\alpha_i \left(T - \frac{[fT]}{f}\right)} - 1 - e^{-\frac{\alpha_i}{f}}}{T \alpha_i \left(1 - e^{-\frac{\alpha_i}{f}}\right)} \right\}, \\
& + \frac{\lambda_d m_1 \Lambda}{(-\rho)} \left\{ 1 + 2[fT] - \frac{[fT]}{fT} ([fT] + 1) - fT \right\} \quad (2.4)
\end{aligned}$$

where  $f$  is pulse repetition frequency and  $[fT]$  represents largest integer less or equal to  $fT$ . The largest  $\alpha_7$  is a prompt-neutron decay constant to be determined and the other  $\alpha_i$  is a decay constant of each delayed-neutron mode. Other notations are conventional except for  $m_1$  and  $m_2$ , which are first and second factorial moment of source multiplicity distribution and are defined by the following equations [8], respectively:

$$m_1 = \bar{N} \overline{v_{\text{sp}}}, \quad (2.5)$$

$$m_2 = \overline{N(N-1)} \overline{v_{\text{sp}}^2} + \bar{N} \overline{v_{\text{sp}}(v_{\text{sp}}-1)}, \quad (2.6)$$

where  $N$  and  $v_{\text{sp}}$  are number of protons in a pulsed bunch and number of neutrons produced by each spallation event, respectively. These definitions lead to the following expression:

$$m_2 - m_1^2 = \left( \overline{N^2} - \bar{N} - \bar{N}^2 \right) \overline{v_{\text{sp}}^2} + \bar{N} \overline{v_{\text{sp}}(v_{\text{sp}}-1)}. \quad (2.7)$$

The above quantity gives an expression for non-Poisson character of a neutron source and is included in the first term of Eq. (2.4). When the proton number  $N$  follows the Poisson distribution, the first term of Eq. (2.7) disappears. The second term is expected to increase with an increase in proton energy but the present energy 100 MeV may lead to a small positive value.

Equation (2.4) is not available for least-squares fitting to the  $Y$  data because of a complexity of the delayed neutron terms and many unknown parameters included in the terms. Here, we reduce the rigorous equation to obtain a practical fitting formula. First, the gate-time  $T$  of the Feynman- $\alpha$  analysis is restricted within the following range:

$$T \ll \frac{1}{\alpha_i} \quad i = 1, 2, \dots, 6. \quad (2.8)$$

In the above range, the following Maclaurin expansions can be done:

$$e^{-\alpha_i T} \simeq 1 - \alpha_i T + \frac{(-\alpha_i T)^2}{2}, \quad (2.9)$$

$$e^{\pm \alpha_i \left( T - \frac{[fT]}{f} \right)} \simeq 1 \pm \alpha_i \left( T - \frac{[fT]}{f} \right) + \frac{1}{2} \alpha_i^2 \left( T - \frac{[fT]}{f} \right)^2, \quad (2.10)$$

$$e^{-\frac{\alpha_i}{f}} \simeq 1 - \frac{\alpha_i}{f}. \quad (2.11)$$

We substitute Eqs. (2.9), (2.10), and (2.11) into Eq. (2.4) to obtain the following final form:

$$\begin{aligned} Y(T) = & C_1 \left( 1 - \frac{1 - e^{-\alpha T}}{\alpha T} \right) \\ & + C_2 \left\{ \frac{e^{-\alpha \left( T - \frac{[fT]}{f} \right)} + e^{-\frac{\alpha}{f}} e^{\alpha \left( T - \frac{[fT]}{f} \right)} - 1 - e^{-\frac{\alpha}{f}}}{T \alpha_p \left( 1 - e^{-\frac{\alpha}{f}} \right)} \right\}, \\ & + C_3 \left\{ 1 + 2[fT] - \frac{[fT]}{fT} ([fT] + 1) - fT \right\} + C_4 T \end{aligned} \quad (2.12)$$

where

$$C_1 = \bar{v}^2 \lambda_d Y_7 \left\{ \lambda_f + \frac{(m_2 - m_1^2) (-\rho)}{m_1 v (v - 1) \Lambda} \right\}, \quad (2.13)$$

$$C_2 = \frac{\bar{v}^2 \lambda_d m_1 (-\rho)}{v (v - 1) \Lambda} Y_7, \quad (2.14)$$

$$C_3 = \frac{\lambda_d m_1 \Lambda}{(-\rho)} - \frac{\bar{v}^2 \lambda_d m_1 (-\rho)}{v (v - 1) \Lambda} \sum_{i=1}^6 Y_i, \quad (2.15)$$

$$C_4 = \bar{v}^2 \lambda_d \sum_{i=1}^6 \frac{Y_i \alpha_i}{2} \left\{ \lambda_f + \frac{(m_2 - m_1^2) (-\rho)}{m_1 v (v - 1) \Lambda} \right\}, \quad (2.16)$$

$$\alpha = \alpha_7. \quad (2.17)$$

In this Feynman- $\alpha$  analysis, Eq. (2.12) is fitted to the  $Y$  data to obtain the prompt-neutron decay constant  $\alpha$  and the four coefficients ( $C_1$ ,  $C_2$ ,  $C_3$ ,  $C_4$ ).

### 2.1.2.2 Rossi- $\alpha$ Formula

In the same manner as a derivation of the practical Feynman- $\alpha$  formula, the Rossi- $\alpha$  formula proposed by Rana and Degweker [6] can be reduced. Their formula can be written as follows:

$$\begin{aligned}
p(\tau) = & \frac{\lambda_d \bar{v}^2}{2} \sum_{i=1}^7 \alpha_i Y_i e^{-\alpha_i \tau} \left\{ \lambda_f + \frac{(m_2 - m_1^2)(-\rho)}{m_1 \bar{v}(\bar{v} - 1) \Lambda} \right\} \\
& + \frac{\lambda_d m_1 \bar{v}^2 (-\rho)}{2 \bar{v}(\bar{v} - 1) \Lambda} \sum_{i=1}^7 \alpha_i Y_i \left\{ \frac{e^{-\alpha_i \left(\tau - \frac{[f\tau]}{f}\right)} + e^{-\frac{\alpha_i}{f}} e^{\alpha_i \left(\tau - \frac{[f\tau]}{f}\right)}}{\left(1 - e^{-\frac{\alpha_i}{f}}\right)} \right\}. \quad (2.18)
\end{aligned}$$

The conditional counting probability  $p(\tau)\Delta\tau$  is a probability that, given a neutron count at a time, there is a subsequent count in  $\Delta\tau$  around time  $\tau$  later. First, the time interval  $\tau$  of the Rossi- $\alpha$  analysis is restricted within the following range:

$$\tau \ll \frac{1}{\alpha_i} \quad i = 1, 2, \dots, 6. \quad (2.19)$$

Under the above time-interval range, the following Maclaurin expansions can be done:

$$e^{-\alpha_i \tau} \simeq 1 - \alpha_i \tau, \quad (2.20)$$

$$e^{\pm\alpha_i \left(\tau - \frac{[f\tau]}{f}\right)} \simeq 1 \pm \alpha_i \left(\tau - \frac{[f\tau]}{f}\right) + \frac{1}{2} \alpha_i^2 \left(\tau - \frac{[f\tau]}{f}\right)^2. \quad (2.21)$$

We substitute the above equations into Eq. (2.18) to obtain the final form:

$$p(\tau) \Delta\tau = C_5 e^{-\alpha \tau} + C_6 \left\{ \frac{e^{-\alpha \left(\tau - \frac{[f\tau]}{f}\right)} + e^{\alpha \left(\tau - \frac{[f\tau]}{f}\right)}}{\left(1 - e^{-\frac{\alpha}{f}}\right)} \right\} + C_7 - C_8 \tau, \quad (2.22)$$

where

$$C_5 = \frac{\lambda_d \bar{v}^2}{2} \alpha_7 Y_7 \left\{ \lambda_f + \frac{(m_2 - m_1^2)(-\rho)}{m_1 \bar{v}(\bar{v} - 1) \Lambda} \right\} \Delta\tau, \quad (2.23)$$

$$C_6 = \frac{\lambda_d m_1 \bar{v}^2 (-\rho)}{2 \bar{v}(\bar{v} - 1) \Lambda} \alpha_7 Y_7 \Delta\tau, \quad (2.24)$$

$$\begin{aligned}
C_7 = & \frac{\lambda_d \bar{v}^2}{2} \sum_{i=1}^6 \alpha_i Y_i \left\{ \lambda_f + \frac{(m_2 - m_1^2)(-\rho)}{m_1 \bar{v}(\bar{v} - 1) \Lambda} \right\} \Delta\tau \\
& + \frac{f \lambda_d m_1 \bar{v}^2 (-\rho)}{\bar{v}(\bar{v} - 1) \Lambda} \sum_{i=1}^6 Y_i \Delta\tau, \quad (2.25)
\end{aligned}$$

$$C_8 = \frac{\lambda_d \bar{v}^2}{2} \sum_{i=1}^6 \alpha_i^2 Y_i \left\{ \lambda_f + \frac{(m_2 - m_1^2)(-\rho)}{m_1 v (v - 1) \Lambda} \right\} \Delta\tau, \quad (2.26)$$

$$\alpha = \alpha_7. \quad (2.27)$$

In this Rossi- $\alpha$  analysis, Eq. (2.22) is fitted to the  $p(\tau)\Delta\tau$  data to obtain the prompt-neutron decay constant  $\alpha$  and the four coefficients ( $C_5, C_6, C_7, C_8$ ).

## 2.1.3 Results and Discussion

### 2.1.3.1 Feynman- $\alpha$ Analyses

Time-sequence counts data within a time interval (gate time) of 1 ms were generated from the arriving time data registered, and then the count data within longer gate times were synthesized by the moving-bunching technique [9] to calculate a gate-time dependence of the  $Y$  defined as variance-to-mean ratio minus 1 of the count's data. Figure 2.3 shows a gate-time  $T$  and a subcriticality dependence of the  $Y$  obtained by the Feynman- $\alpha$  analysis, where neutron counter is B1. The gate-time dependence of the  $Y$  is oscillatory due to the periodicity of the pulsed source. The  $Y$  of the slightly subcritical pattern B tends to increase with a lengthening in gate time, while that of the deeply subcritical patterns C, D, and E scarcely have the increasing trend and the difference of the amplitude among these patterns is small. At pattern F, whose  $Y$  is not drawn in Fig. 2.3, the  $Y$  scarcely has the increasing trend and the amplitude is slightly smaller than that at pattern E. The least-squares fits of Eq. (2.12) to the  $Y$  data are included in Fig. 2.3, where the fitted curves are in very good agreement with the  $Y$  data. The result obtained from counter B2 and B3 was similar to the above observation obtained from counter B1 but that from counter B4 was entirely different.

**Fig. 2.3** Subcriticality dependence of  $Y$  value of counter B1 (Ref. [1])

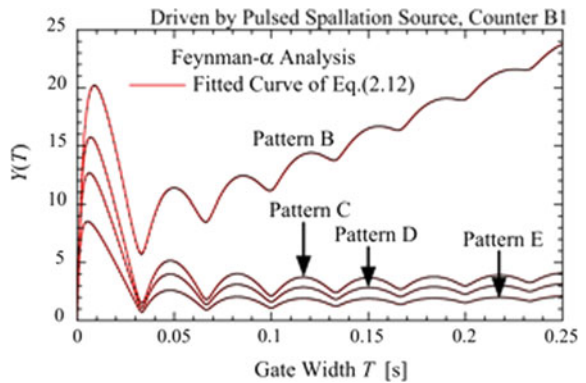




**Fig. 2.4** Subcriticality dependence of Y value of counter B4 (Ref. [1])

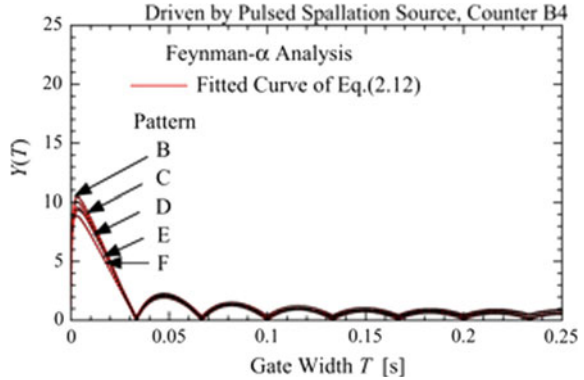
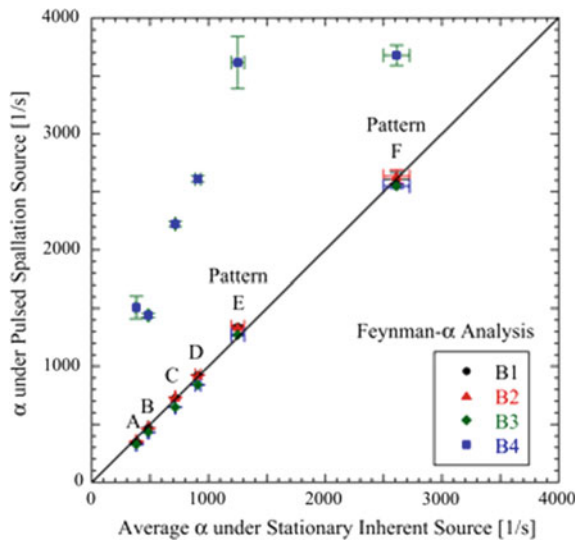


Figure 2.4 shows a gate-time  $T$  and a subcriticality dependence of the  $Y$  obtained by the Feynman- $\alpha$  analysis, where neutron counter is B4. In a shorter gate-time range than about 0.03 s, a slight difference in the  $Y$  among subcritical patterns can be observed. In the longer range, however, the  $Y$  data of respective patterns are overlapped. This feature suggests that counter B4 hardly detects fission neutrons which have an information of the subcriticality and most of the neutron counts must be generated from the detection of source neutrons arriving from the target.

In Fig. 2.5, the prompt-neutron decay constant  $\alpha_p$  obtained from the present Feynman- $\alpha$  analysis under the pulsed spallation source is compared with the average decay constant done from the previous analysis under a stationary source inherent in nuclear fuels [2], where the previous three decay constants from three neutron counters (B1, B2, B3) are averaged to obtain the average and the standard deviation.

**Fig. 2.5** Comparison of respective prompt neutron decay constants obtained from Feynman- $\alpha$  analyses under pulsed spallation and stationary inherent source (Ref. [1])



The error of the present decay constant represents statistical uncertainty  $\pm 1\sigma$  derived from a nonlinear least-squares method. Since counter B4 was placed far from the core and consequently had very small detection efficiency, the previous analysis for the counter was unsuccessful.

The present decay constants of counters B1, B2, and B3 agree well with the previous average decay constant, while the decay constant of counter B4 is much larger than the previous one. As mentioned in Fig. 2.4, the counter B4 placed far from the fuel region and closely to the target must scarcely detect fission neutrons and consequently have little information about fission chain. Most of neutron counts of the counters B1, B2, and B3 located closely to the fuel region are expected to be generated from the detection of fission neutrons.

### 2.1.3.2 Rossi- $\alpha$ Analyses

Figure 2.6 shows a time-interval  $\tau$  and subcritical-pattern dependences of the conditional counting probability  $p(\tau)\Delta\tau$  obtained by the Rossi- $\alpha$  analysis, where neutron counter is B1. The least-squares fits of Eq. (2.22) to the counting probability data are included in this figure, where the fitted curves seem to be in good agreement with the data but the fittings are unsuccessful. Figure 2.7 shows an enlarged view near the second peak in Fig. 2.6. A considerable difference between the counting probability data and Eq. (2.22) fitted to the data can be observed. The probability data have a smooth convex top at every integral multiple of pulse period, while the fitted curve of Eq. (2.22) has a sharp cusp arising from a delta-function-like shape of pulsed neutron. Since the pulse width of 100 ns of our accelerator is much shorter than the time scale of the present correlation analyses, the assumption that each pulse has a delta-function-like shape is acceptable. Here, we consider the reason why the Rossi- $\alpha$  data had the smooth convex top.

In the previous pulsed-neutron-source experiments [10–12], a considerable delay in counter response to neutron generation has been observed. The delay has been considered to originate primarily from a slowing down and a thermalization time of

**Fig. 2.6** Subcriticality dependence of  $P(\tau)\Delta\tau$  of counter B1 (Ref. [1])

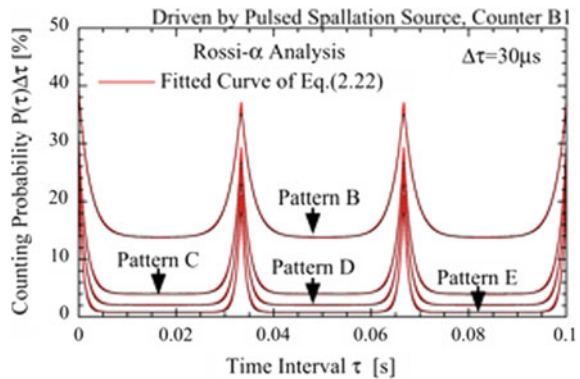
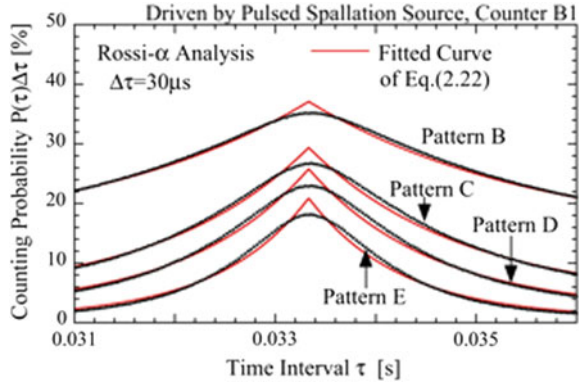


**Fig. 2.7** Enlarged view near a peak in Fig. 2.6 (Ref. [1])



high-energy source neutrons for moderation to thermal energy and from a diffusion time of the thermalized source neutrons for arrival at core. The delay could be also interpreted as a higher harmonics effect [13, 14].

In the previous pulsed-neutron-source experiments mentioned above, the decay data deviated from a single exponential curve were masked to determine the fundamental prompt-neutron decay constant from a least-squares fitting of a conventional formula based on the one-point kinetics model. We tried to apply this masking technique to the present Rossi- $\alpha$  analysis. As shown in Fig. 2.8, the data around each smooth convex top were masked for a least-squares fitting of the present Rossi- $\alpha$  formula. The cusps of these fitted curves appear sharper than those of Fig. 2.7. The correlation coefficient is an indication of a goodness of the least-squares fitting. In this study, we employed the mask width with the maximum coefficient. The optimal mask width for every counter and every subcritical pattern was determined.

In Fig. 2.9, the prompt-neutron decay constant  $\alpha$  obtained from the present Rossi- $\alpha$  analysis under the pulsed spallation source is compared with the average decay constant done from the previous analysis under a stationary source inherent in nuclear fuels [2], where the masking technique is not applied to the present analysis. The

**Fig. 2.8** Masking data around peaks for least-squares fitting (Ref. [1])

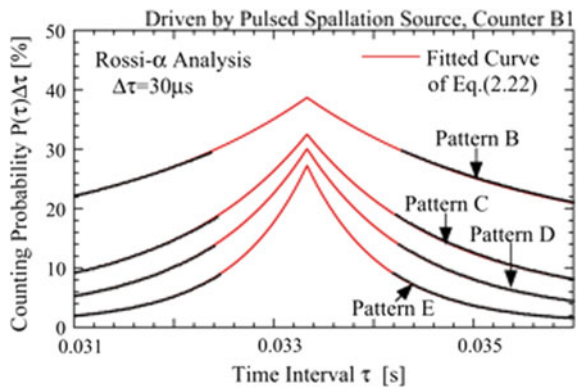
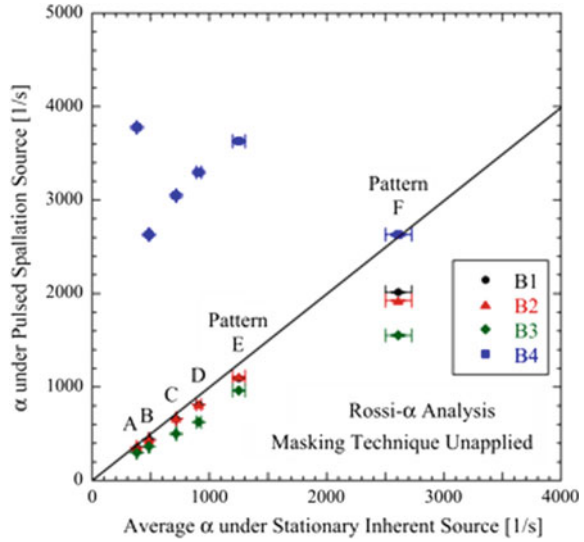
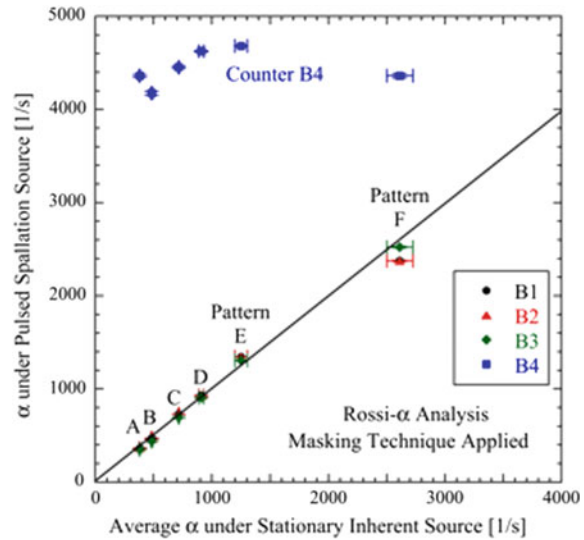


**Fig. 2.9** Comparison of respective prompt-neutron decay constants obtained from Rossi- $\alpha$  analyses under pulsed spallation and inherent source (Ref. [1])



present decay constant is in poor agreement with the previous one. This disagreement could be resolved by applying the masking technique, as shown in Fig. 2.10. Except for counter B4, the decay constant obtained from the present analysis with the masking technique is in good agreement with that done from the previous analysis. The counter B4 placed far from the fuel region and closely to the neutron source derives a large decay constant of source neutrons in reflector. As shown in Fig. 2.5, the decay constant obtained from the present Feynman- $\alpha$  analysis, except for counter

**Fig. 2.10** Effect of masking data around peaks on prompt-neutron decay constant obtained from Rossi- $\alpha$  analysis under pulsed spallation source (Ref. [1])



B4, well agreed with the previous decay constant. We can have this fortunate agreement because the respective negative and positive sharp cusps of the uncorrelated second and third terms of Eq. (2.12) barely cancel out, as shown in Fig. 2.5. In contrast, the present Rossi- $\alpha$  formula has no cancelation mechanism and has sharp cups at every integral multiple of pulse period.

### 2.1.3.3 Comparison of Correlation Amplitude Between Spallation and Poisson Sources

Many authors [6, 8, 15–18] theoretically showed that the non-Poisson spallation source enhanced the correlation amplitudes of various reactor noise analyses. Here, we compare the correlation amplitudes obtained from the Feynman- $\alpha$  and Rossi- $\alpha$  analyses under the present non-Poisson spallation source with those under the previous Poisson inherent source [2]. First, the respective prompt correlation amplitudes  $C_1$  and  $C_5$  of the present Feynman- $\alpha$  and Rossi- $\alpha$  formulae are rewritten in the familiar forms. The prompt quantity  $Y_7$  included in the correlation amplitudes can be described as follows [6]:

$$Y_7 = \frac{\overline{v(v-1)}}{\bar{v}^2 \alpha^2}. \quad (2.28)$$

When the above equation is substituted for Eqs. (2.13) and (2.23), the following equations can be, respectively, obtained:

$$C_1 = \lambda_d \frac{\overline{v(v-1)}}{\alpha^2} \left\{ \lambda_f + \frac{(m_2 - m_1^2)(-\rho)}{m_1 \overline{v(v-1)} \Lambda} \right\}, \quad (2.29)$$

and

$$C_5 = \frac{\lambda_d \overline{v(v-1)}}{2\alpha} \left\{ \lambda_f + \frac{(m_2 - m_1^2)(-\rho)}{m_1 \overline{v(v-1)} \Lambda} \right\} \Delta\tau. \quad (2.30)$$

The respective correlation amplitudes  $C_{1P}$  and  $C_{5P}$  of the conventional Feynman- $\alpha$  and Rossi- $\alpha$  formulae for a stationary Poisson source can be described as follows [7]:

$$C_{1P} = \lambda_d \lambda_f \frac{\overline{v(v-1)}}{\alpha^2}, \quad (2.31)$$

and

$$C_{5P} = \frac{\lambda_d \lambda_f \overline{v(v-1)}}{2\alpha X_P} \Delta\tau, \quad (2.32)$$

where

$$\lambda_d = \varepsilon \lambda_f. \tag{2.33}$$

Assuming that a detection efficiency  $\varepsilon$  has no difference between the non-Poisson spallation and the Poisson sources, the following relationships hold:

$$C_1 = C_{1P} + \frac{\lambda_d (m_2 - m_1^2) (-\rho)}{m_1 \alpha^2 \Lambda}, \tag{2.34}$$

and

$$C_5 = C_{5P} + \frac{\lambda_d (m_2 - m_1^2) (-\rho)}{2 m_1 \alpha \Lambda} \Delta\tau. \tag{2.35}$$

The respective second terms of the right-hand sides of the above two equations express the enhancement by the non-Poisson character of the spallation source. The enhancement disappears at a critical state and increases with an increase in subcriticality.

Next, the subcriticality dependence of the enhancement is experimentally confirmed. Figure 2.11 shows a comparison of respective prompt correlation amplitudes obtained from the Feynman- $\alpha$  analyses under the present pulsed spallation and the stationary inherent sources. The latter is a stationary Poisson source since the inherent source neutrons are dominantly produced by  $(\alpha, n)$  reaction and spontaneous fissions negligibly contribute to the source strength [2]. This figure indicates

**Fig. 2.11** Comparison of respective prompt-neutron correlation amplitudes obtained from Feynman- $\alpha$  analyses under pulsed spallation and stationary inherent sources (Ref. [1])

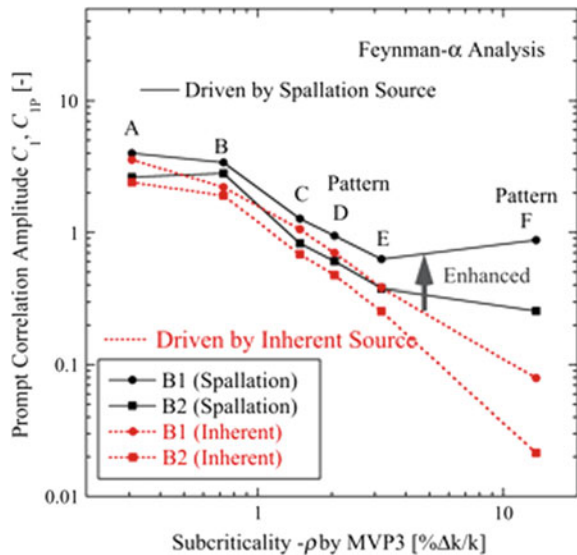
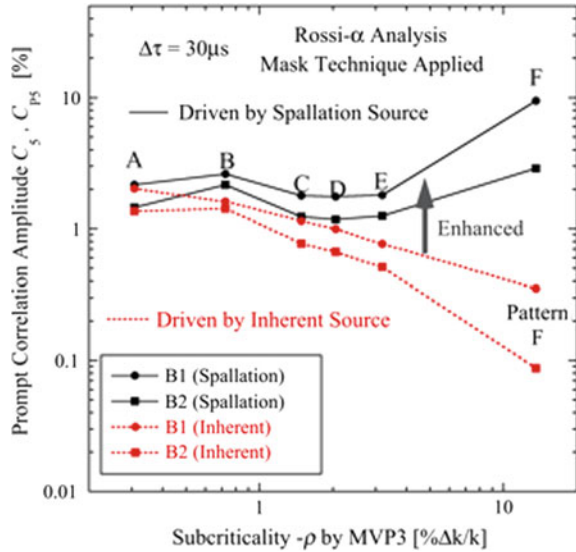


**Fig. 2.12** Comparison of respective prompt-neutron correlation amplitudes obtained from Rossi- $\alpha$  analyses under pulsed spallation and stationary inherent sources (Ref. [1])



that the enhancement of the prompt correlation amplitude increases with an increase in subcriticality. The non-Poisson character of the spallation source enhances the amplitude clearly.

Figure 2.12 also shows another comparison of respective prompt correlation amplitudes obtained from the Rossi- $\alpha$  analyses under the present pulsed spallation and the stationary inherent sources. This also indicates that the non-Poisson character of the spallation source significantly enhances the amplitude. The above discussion is confined to the qualitative observation and some quantitative evaluation of the non-Poisson character must be difficult. This is because a detection efficiency  $\varepsilon$  has a considerable difference between the external spallation and the inherent sources and the efficiency must depend on the subcriticality. A spatially uniform inherent source in fuels hardly excites any higher modes, however, another spatially localized external source significantly excites a higher mode with an increase in subcriticality, as could be observed in a source multiplication measurement [2]. In next Sect. 2.1.3.4, we try to derive a quantitative indicator of the non-Poisson character.

#### 2.1.3.4 Indicator of Non-poisson Character of Spallation Source

Dividing Eq. (2.23) by Eq. (2.24) of the present Rossi- $\alpha$  formula, the following equation can be obtained:

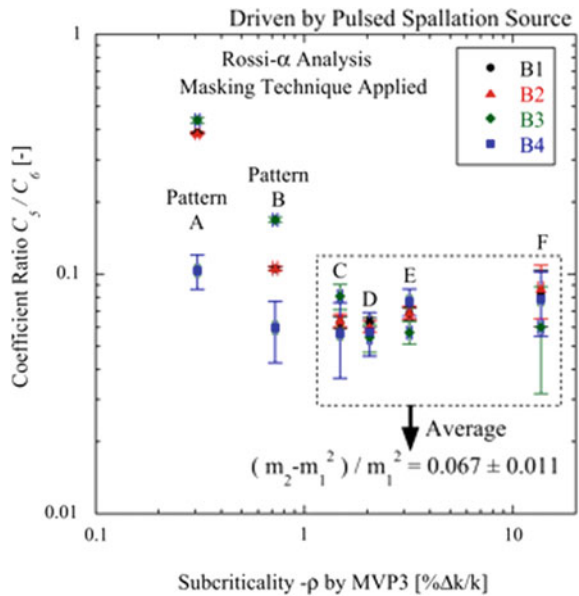
$$\frac{C_5}{C_6} = \frac{\lambda_f \overline{v(v-1)} \Lambda}{m_1(-\rho)} + \frac{m_2 - m_1^2}{m_1^2}. \quad (2.36)$$

The above equation has no detection efficiency and asymptotically approaches the second term with an increase in the subcriticality. The second term quantitatively expresses a non-Poisson character of the spallation source and may be referred to as “the Degweker’s factor” of multiplicity distribution of neutrons in a pulse bunch. When the multiplicity follows the Poisson distribution, the factor becomes zero. Degweker et al. theoretically simulated the Rossi- $\alpha$  analysis changing parametrically the above factor to investigate an impact of non-Poisson source [8].

Generally, the ratio of the second factorial moment to the first factorial moment squared of a multiplicity distribution has been employed as an indication characterizing the distribution. As an example, Diven factor [19] is defined as the ratio of the second factorial moment to the first factorial moment squared of a multiplicity distribution of fission neutrons emitted from a fission event and is a useful indication characterizing the multiplicity distribution. Adding 1 to the Degweker’s factor, the result is the ratio of the second factorial moment to the first factorial moment squared of the multiplicity distribution of neutrons in a pulse bunch. Consequently, this factor is eligible to employ as the indication characterizing the multiplicity distribution and should be determined experimentally.

Figure 2.13 shows a subcriticality dependence of the ratio  $C_5/C_6$  determined from the present Rossi- $\alpha$  analysis. At the more deeply subcritical system than pattern C, the ratio seems to be an asymptotic value. Seeing the ratio within the subcritical range from pattern C to F, no systematic dependence on the subcriticality can be observed. Averaging the ratios over the subcritical range and over four counters, we obtain the second term, i.e., the Degweker’s factor of  $0.067 \pm 0.011$ . The non-zero value convinces us that the present spallation source has the non-Poisson character.

**Fig. 2.13** Subcriticality dependence of coefficient ratio  $C_5/C_6$  obtained from Rossi- $\alpha$  analysis (Ref. [1])





If the accelerator had higher energy proton beam than 100 MeV, the factor would be larger [20].

## 2.2 Power Spectral Analyses

### 2.2.1 Experimental Settings

The power spectral analysis on frequency domain is carried out in the same A-core as shown in Fig. 2.2 [21]. Figure 2.14 shows the present signal processing circuit, whose former stage consisted of conventional charge preamplifier (PA), detector bias-supply (HV), spectroscopy amplifier (SA), and single-channel analyzer (SCA) modules. A special count-rate meter (Oken S-1955) input logic pulse train from SCA to output analog signal proportional to instantaneous count rate. The rate meter could be well modeled by a primary delay element which had the time constant of 3.88 ms (break frequency 41.0 Hz). The time constant of the meter is so short that a large portion of reactor noise passes through the filtration. Finally, analog signals from the two count-rate meters were fed to a fast Fourier transform (FFT) analyzer (Ono DS-3200) to obtain auto- and cross-power spectral densities and to record the analog signals as digital data. This FFT analyzer has a highly resolvable analog-to-digital converter whose number of bits and dynamic range are 24 bits and above 110 dB, respectively. An analysis range in frequency from 1.25 to 1000 Hz was specified to obtain 800-point spectral data. Delayed neutrons are expected to contribute hardly to the power spectral density obtained from the FFT analyzer because the above minimum frequency of 1.25 Hz is larger than the 6th decay constant  $3.01 \text{ s}^{-1}$  (0.48 Hz) of a delayed neutron data given by Keepin [22].

In each subcritical pattern, time-sequence signal data were acquired for about 10 min. A response function of the above count-rate meter was measured in advance and the auto-and cross-power spectral densities obtained were divided by the auto-power spectral density of the response of the count-rate meter, so as to compensate an influence of the meter. Throughout the present accelerator operations, the pulsed

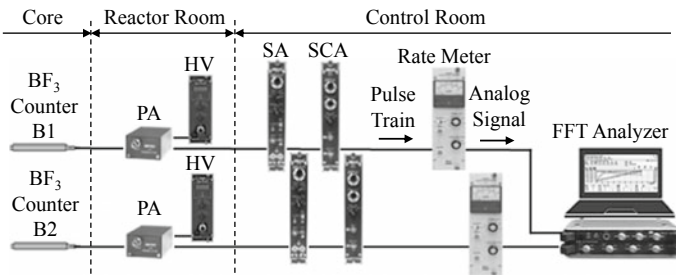


Fig. 2.14 Signal processing circuit for power spectral analysis (Ref. [21])

repetition frequency and the beam width were set to 30 Hz and 100 ns, respectively. The proton beam intensity of an accelerator was set to 30 pA.

## 2.2.2 Formula for Power Spectral Analyses

### 2.2.2.1 Degweker's Formula

Degweker and Rana [8] formulated the auto- and cross-power spectral densities for a periodically pulsed non-Poisson source, where delayed neutron contribution was neglected and each pulse was assumed to be a delta function. The neglect of delayed neutron contribution is acceptable as mentioned in the above Sect. 2.2.1. Since the pulse width 100 ns of our accelerator is much shorter than the time scale of the present analysis, the assumption of the delta function is also acceptable. Here, their formulae are rewritten as a function of not angular frequency  $\omega$  s<sup>-1</sup> but frequency  $f$  Hz. Then, their cross-power spectral density between neutron detector 1 and 2 can be described as follows:

$$\Phi_{12}(f) = \frac{C_1(f)}{(2\pi f)^2 + \alpha^2} + C_2(f) \sum_{n=-\infty}^{\infty} \frac{\delta(f - n f_R)}{(2\pi f)^2 + \alpha^2}, \quad (2.37)$$

where

$$C_1(f) = H(f) q^2 f_R \lambda_{d1} \lambda_{d2} (m_2 - m_1^2 + 2m_1 Y_1), \quad (2.38)$$

$$C_2(f) = H(f) q^2 f_R^2 \lambda_{d1} \lambda_{d2} m_1^2, \quad (2.39)$$

$$Y_1 = \lambda_f \frac{\overline{v(v-1)}}{2\alpha}. \quad (2.40)$$

Their auto-power spectral density of neutron detector 1 can be also described as follows:

$$\Phi_{11}(f) = C_3(f) + \frac{C_4(f)}{(2\pi f)^2 + \alpha^2} + C_5(f) \sum_{n=-\infty}^{\infty} \frac{\delta(f - n f_R)}{(2\pi f)^2 + \alpha^2}, \quad (2.41)$$

where

$$C_3(f) = \frac{H(f) q^2 f_R \lambda_{d1} m_1}{\alpha}, \quad (2.42)$$

$$C_4(f) = H(f) q^2 f_R \lambda_{d1}^2 (m_2 - m_1^2 + 2m_1 Y_1), \quad (2.43)$$

$$C_5(f) = H(f) q^2 f_R^2 \lambda_{d1}^2 m_1^2, \quad (2.44)$$

where  $\alpha$  and  $f_R$  represent prompt-neutron decay constant and pulse repetition frequency, respectively.  $H(f)$  is a power spectral density of an impulse response of detector and processing-circuit system.

### 2.2.2.2 Formula Applied to Present Analyses

The auto-power spectral density has a white chamber noise indicated by the first term of Eq. (2.41). The correlated component done by the second term is completely hidden by the chamber noise in a higher frequency range, and this feature suggests a difficulty in estimating the break frequency, i.e., the prompt-neutron decay constant [12, 23]. In previous reactor noise analysis for a stationary source, Nomura [24] proposed the use of two neutron detectors with independent electronic circuits to reduce this spurious white noise and demonstrated the usefulness of his proposal. His original improvement referred to as the two-detector method is identical with the cross-power spectral analysis familiar to signal processing field. Actually, Eq. (2.37) for the cross-power spectral density has no term of the white noise. In the present study, we analyze only the cross-power spectral density free from the white noise.

The two coefficients defined by Eqs. (2.38) and (2.39) include  $H(f)$  and depend on frequency  $f$ . When the frequency response of the count-rate meter is compensated as mentioned in Sect. 2.2.1, these coefficients are independent of the frequency. For the following expressions, each coefficient is described as a constant. Then, Eq. (2.37) can be rewritten as

$$\Phi_{12}(f) = \frac{C_1}{(2\pi f)^2 + \alpha^2} + C_2 \sum_{n=-\infty}^{\infty} \frac{\delta(f - n f_R)}{(2\pi f)^2 + \alpha^2}. \quad (2.45)$$

The second term of the above equation gives an expression to the uncorrelated delta-function peaks at the multiple of pulse repetition frequency  $f_R$ . At frequency of the integral multiple, Eq. (2.45) can be reduced as follows:

$$\Phi_{12}(n f_R) = \frac{C_1}{(2\pi n f_R)^2 + \alpha^2} + \frac{C_2}{(2\pi n f_R)^2 + \alpha^2}, \quad n = 1, 2, 3, \dots \quad (2.46)$$

The second uncorrelated term of the above equation is larger than the first correlated term by over two orders of magnitude [12, 23]. Then, Eq. (2.46) can be simplified as

$$\Phi_{12}(n f_R) \simeq \frac{C_1}{(2\pi n f_R)^2 + \alpha^2}, \quad n = 1, 2, 3, \dots \quad (2.47)$$

From a least-squares fit of Eq. (2.47) to peak data at frequency of the integral multiple of  $f_R$ , the prompt-neutron decay constant  $\alpha$  and coefficient  $C_2$  can be determined.

Next, a well-known effect of a higher mode excited by the injection of pulsed neutrons [10–12] should be considered. Sakon et al. employed the following equation to consider the effect successfully [12, 23].

$$\Phi_{12}(n f_R) \simeq \frac{C_2}{(2\pi n f_R)^2 + \alpha^2} + \frac{C_{2H}}{(2\pi n f_R)^2 + \alpha_H^2}, \quad n = 1, 2, 3, \dots \quad (2.48)$$

When certain a higher prompt mode as well as a fundamental prompt mode are excited, such a higher term as the second term of the above equation can be added to the fundamental term of the power spectral density [25–27]. The prompt-neutron decay constant of the higher mode is represented by  $\alpha_H$ . The coefficient  $C_{2H}$  includes the eigenfunction and the adjoint eigenfunction of the higher prompt mode. We try to apply Eq. (2.48) as well as Eq. (2.47) to derive the fundamental decay constant  $\alpha$  from the uncorrelated peaks.

When the uncorrelated peaks of the cross-power spectral density are masked, Eq. (2.45) can be reduced to the following equation for the remaining data unmasked:

$$\Phi_{12}(f) = \frac{C_1}{(2\pi f)^2 + \alpha^2}. \quad (2.49)$$

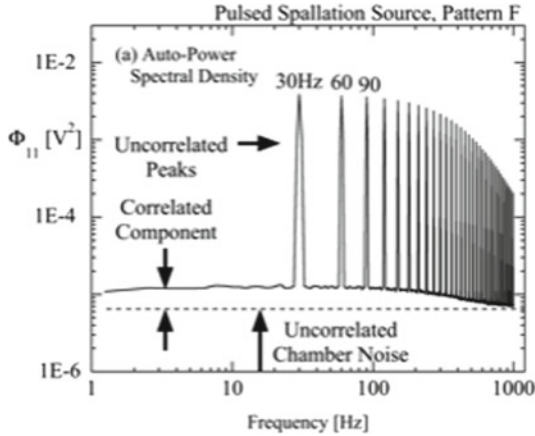
From a least-squares fit of Eq. (2.49) to the unmasked data, the prompt neutron decay constant  $\alpha$  and coefficient  $C_1$  can be also determined. The above equation gives an expression to the correlated noise component and is identical to the familiar formula for a stationary neutron source.

## 2.2.3 Results and Discussion

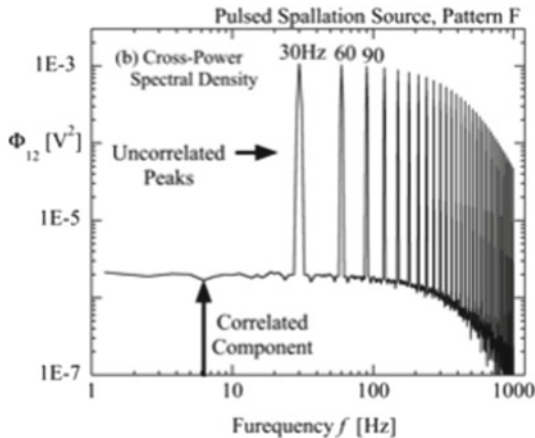
### 2.2.3.1 Power Spectral Density

Figure 2.15a, b show measured auto-power spectral density of counter B1 and cross-power spectral density between neutron detector B1 and B2, respectively, where subcritical pattern is F. The auto-power spectral density is composed of a continuous correlated component, another constant chamber noise and many delta-function-like peaks at the integral multiple of the repetition frequency, as expected by Eq. (2.41). The correlated component tends to be hidden by the white chamber noise with an increase in frequency and this feature suggests a difficulty in estimating the break frequency, i.e., the prompt-neutron decay constant.

On the other hand, the cross-power spectral density has no white chamber noise, expected by Eq. (2.37). The correlated component is larger than one decade (20 dB). This feature is significantly different from that of the auto-power spectral density as



(a) Auto-power spectral density of counter B1



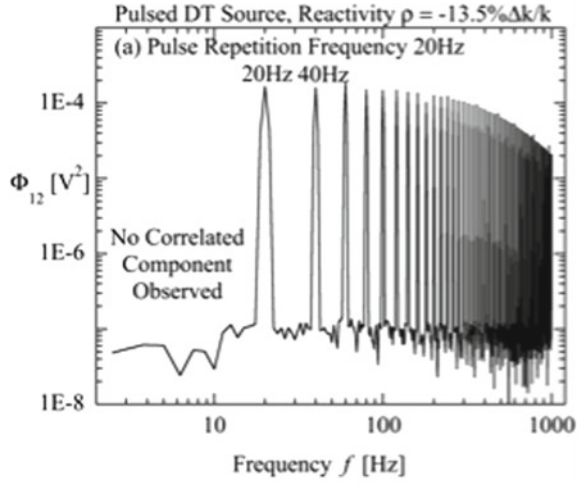
(b) Cross-power spectral density between counters B1 and B2

**Fig. 2.15** Power spectral density measured at subcritical pattern F (Ref. [21])

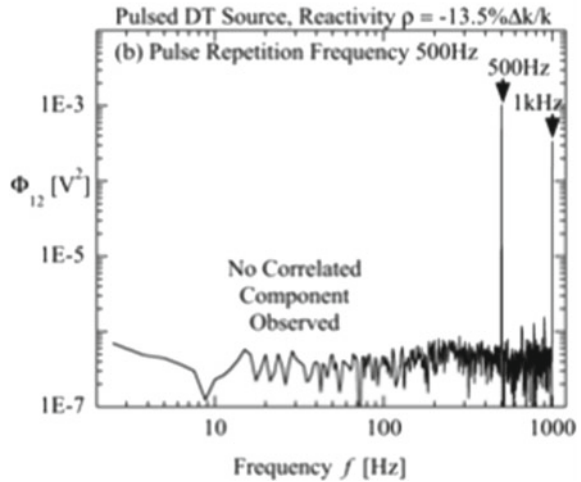
shown above. Obviously, the cross-power spectral density is favorable to estimating the decay constant.

For almost the same subcritical system driven a pulsed 14 MeV Poisson source, previously, a power spectral analysis was carried out [12]. Figure 2.16a, b show the cross-power spectral densities measured previously, where the respective pulse repetition frequencies are 20 and 500 Hz and the subcriticality  $13.59 \% \Delta k/k$  is almost same as that of the present pattern F. In these cross-power spectral densities, no correlated noise component could be observed, and we failed in determining the prompt-neutron decay constant from correlated component. Naturally, the auto-power spectral density also had no correlated component. In contrast to the previous analysis, the present analysis gives a considerable correlated component as shown

**Fig. 2.16** Cross-power spectral density measured previously at a subcritical KUCA system driven by a pulsed DT neutron source (Ref. [21])



(a) Pulse repetition frequency 20 Hz



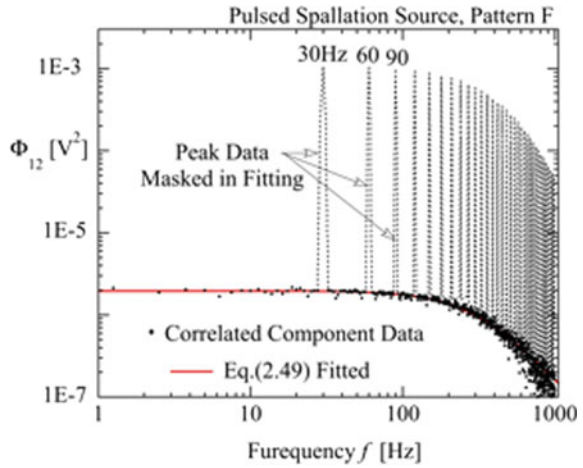
(b) Pulse repetition frequency 500 Hz

in Fig. 2.15. The non-Poisson character of the spallation source must enhance the amplitude of the correlated component over a precision limit of the FFT analyzer.

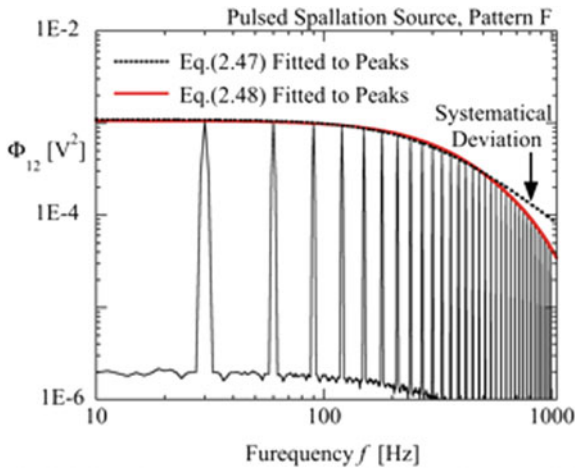
### 2.2.3.2 Prompt Neutron Decay Constant

Figure 2.17 shows a least-squares fit of Eq. (2.49) to the correlated noise component of the cross-power spectral density measured at pattern F. In this fitting, 33 delta-function-like peaks were masked. No systematical deviation of the fitted curve from the data can be seen. Figure 2.18 shows a least-squares fit of Eqs. (2.47) and (2.48)

**Fig. 2.17** Least-squares fit to correlated component of cross-power spectral density (Ref. [21])



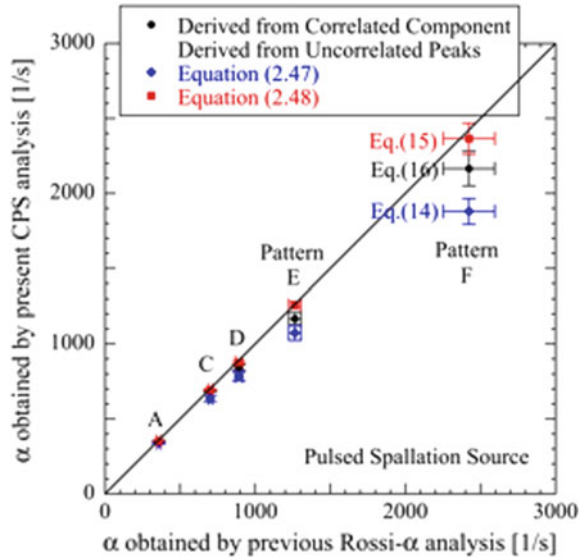
**Fig. 2.18** Least-squares fit to uncorrelated peaks of cross-power spectral density (Ref. [21])



to the peak points of the cross-power spectral density at pattern F. No systematical deviation of fitted Eq. (2.47) from the peak point can be seen in a lower frequency range than roughly 500 Hz, while above this frequency, a systematical deviation of the fitted curve from the peak points is significant. In contrast to Eq. (2.47), no deviation of fitted Eq. (2.48) from the peaks can be observed over the frequency range. At all subcritical patterns, the fittings of Eq. (2.48) were very successful.

In Fig. 2.19, the prompt-neutron decay constant obtained from the present cross-power spectral analysis is compared with the average decay constant done from the previous Rossi- $\alpha$  analysis under the same spallation source [1]. When Eq. (2.47) is fitted to uncorrelated peaks, the present decay constant is in poor agreement with the previous one. Fortunately, the fitting of Eq. (2.48) completely resolves this disagreement. When Eq. (2.49) is fitted to continuous correlated data, the agreement with

**Fig. 2.19** Comparison of respective prompt neutron decay constants obtained from present cross-power spectral and previous Rossi- $\alpha$  analyses (Ref. [21])



the previous decay constant is not too bad. The analysis for a much longer time than 10 min may be required to enhance the agreement.

**2.2.3.3 Indicator of Non-poisson Character of Spallation Source**

Dividing Eq. (2.38) by Eq. (2.39) of the formula for cross-power spectral density, the following equation can be obtained:

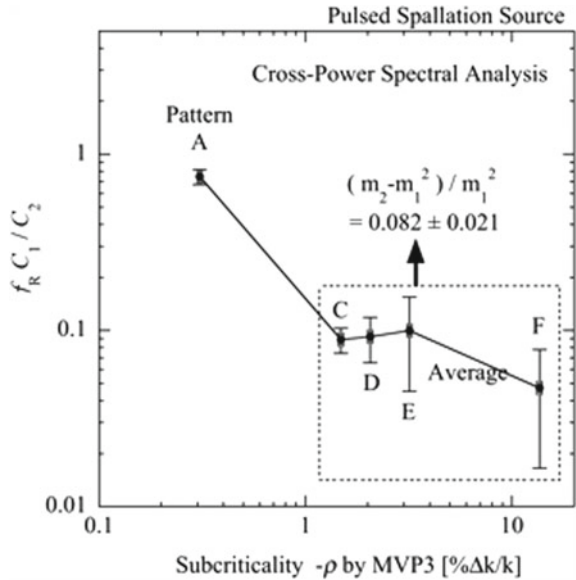
$$f_R \frac{C_1}{C_2} = \frac{\lambda_f \overline{v(v-1)}}{m_1 \alpha} + \frac{m_2 - m_1^2}{m_1^2}. \tag{2.50}$$

The above equation has no detection efficiency and asymptotically approaches to the second term with an increase in the subcriticality, i.e., the prompt-neutron decay constant  $\alpha$ . The second term quantitatively expresses a non-Poisson character of the spallation source and may be referred to as “the Degweker’s factor” of multiplicity distribution of neutrons in a pulse bunch. When the multiplicity follows the Poisson distribution, the factor becomes zero. Degweker et al. theoretically simulated the Rossi- $\alpha$  analysis changing parametrically the above factor to investigate an impact of non-Poisson source [8]. The Degweker’s factor is a useful indication characterizing the multiplicity distribution of the spallation neutrons in a pulsed bunch.

Figure 2.20 shows a subcriticality dependence of the ratio  $f_R C_1/C_2$  determined from the present cross-power spectral analysis. At the more deeply subcritical system than pattern C, the ratio seems to be an asymptotic value. Seeing the ratio within the subcritical range from pattern C to F, no systematic dependence on the subcriticality



**Fig. 2.20** Subcriticality dependence of  $f_R C_1/C_2$  (Ref. [21])



can be observed and these ratios are considered to be the asymptotic value, i.e., the Degweker’s factor. Averaging the ratios over the subcritical range from Pattern C to F, we obtained the second term, i.e., the Degweker’s factor of  $0.082 \pm 0.021$ . This value is consistent with  $0.067 \pm 0.011$  determined from the previous Rossi- $\alpha$  analysis [1].

## 2.3 Beam Trip and Restart Methods

### 2.3.1 Experimental Settings

#### 2.3.1.1 Core Configurations

A series of accelerator-beam trip and restart experiments is carried out to determine the subcriticality of a reactor system driven by a pulsed 14 MeV neutron source [28]. This core configuration is shown in Fig. 2.21. The core was composed of 20 regular fuel assemblies and one partial fuel assembly, which were loaded on the grid plate. The fuel and moderator elements of each assembly were set in a 1.5-mm-thick aluminum sheath and the cross section of the elements within the assembly was the square of 2”. The regular fuel assembly was composed of 36 unit cells of one (1/16” thick) uranium plate with Al clad and two (1/8” and 1/4” thick) polyethylene plates, while the partial fuel assembly was composed of 12 unit cells of these plates. The partial fuel assembly was employed to adjust the excessive reactivity of the core.

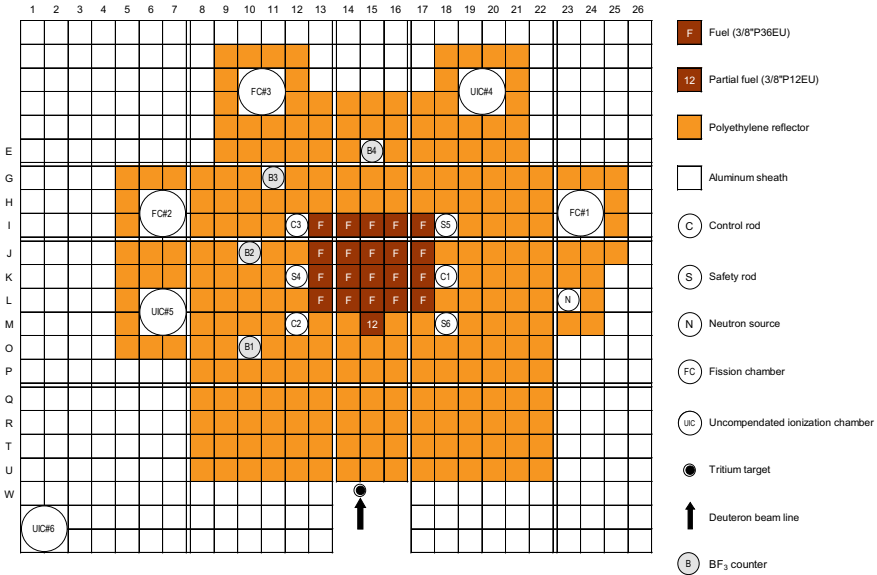


**Fig. 2.21** Top view of core configuration and neutron detector location (Ref. [28])

The active height of the core was about 40 cm, with additional about 60 cm upper and lower polyethylene reflectors. The configuration of these fuel assemblies was reported in detail by Pyeon et al. [29].

A pulsed neutron generator was combined with the core, where 14 MeV pulsed DT neutrons were injected into the subcritical system through the polyethylene reflector. The generator consisted of a duoplasmatron-type ion source, a Cockcroft-Walton-type accelerator for deuteron ( $D^+$ ) beam, and tritium (T) target of gas-in-metal type. The pulsed neutrons are generated through the D-T reaction by the pulsed and accelerated  $D^+$  beam and T in the target metal. The target was placed outside the polyethylene reflector, as shown in Fig. 2.21. The pulse duration and repetition period of the  $D^+$  beam pulse can be remotely controlled by using an arc-pulsar installed in the control room of KUCA. The current and acceleration voltage of the  $D^+$  beam pulse can also be controlled from the control room. In the present experiment, the major parameters of the accelerator drive were set to 160 keV in beam energy, 0.6–0.8 mA in beam current, 0.8 ms in pulse width, 1 ms in pulse repetition period, and 5.1–9.2 V in arc voltage of the ion source.

**2.3.1.2 Experimental Procedures and Conditions**

Four  $BF_3$  proportional counters (1" dia.) were employed as experimental channels. As shown in Fig. 2.21, these  $BF_3$  counters were placed on several positions around the core to measure the reactor response to beam trip and restart operations and to

**Table 2.2** Control rod patterns employed in the present experiment (Ref. [28])

Pattern	Rod position			Reactivity
	C1	C2, C3	S4, S5, S6	[% $\Delta k/k$ ]
A	L.L.	U.L.	U.L.	-0.240
B	L.L.	L.L.	U.L.	-0.636
C	L.L.	L.L.	L.L.	-1.577

L.L.: Lower Limit [0 mm], U.L.: Upper Limit [1200 mm]

investigate the spatial dependence. The nuclear instrumentation system consisted of a detector bias supply, a preamplifier, a spectroscopy amplifier, and discriminator modules. Finally, signal pulses from four neutron counters were fed to a multichannel scaler to acquire time-sequence count data. The gate width of the scaler was set to 0.1 s. At a slightly subcritical state, the count rate of each neutron counter was expected to be so high that count losses would be induced by the dead-time effect of the neutron counter. Hence, the acquired count data were corrected for the losses on the basis of the non-paralysable model, where we used the dead time of 4  $\mu$ s predetermined by an improved Feynman- $\alpha$  analysis [30].

First, an Am-Be neutron source for reactor startup was inserted. Then, the subcriticality for the experiment was adjusted by changing the axial positions of safety rods and control ones. The neutron source was taken out of the core and the injection of pulsed neutrons began. The control rod patterns employed in the experiment are shown in Table 2.2. The reference reactivity, included in this table, was evaluated from the reactivity worth of each rod, whose worth was predetermined by the positive period method and the rod drop one.

In a beam trip experiment, a certain arc voltage of the ion source was suddenly dropped to turn off the D<sup>+</sup> pulse beam. In the succeeding beam restart experiment, the voltage was rapidly returned to the original value to turn on the beam.

## 2.3.2 Data Analyses Method

### 2.3.2.1 Least-Squares Inverse Kinetics Method

First, the theory of the least-squares inverse kinetics method (LSIKM) [31–33] is briefly described. Assuming the zero-power and one-point kinetics model, the time-dependent neutron behavior of a subcritical reactor system driven by an external neutron source can be described as

$$\frac{dN(t)}{dt} = \frac{\rho - \beta}{\Lambda} N(t) + \sum_{k=1}^6 \lambda_k C_k(t) + S, \quad (2.51)$$

$$\frac{dC_k(t)}{dt} = \frac{\beta_k}{\Lambda} N(t) - \lambda_k C_k(t), \quad (2.52)$$

where  $N(t)$  is the neutron density,  $C_k(t)$  the concentration of  $k$ -th-group precursor, and  $S$  the neutron source strength. Other notations are conventional. As the above neutron density, usually, time-sequence count-rate data can be employed to determine the reactivity  $\rho$ . The differential term of Eq. (2.51) is usually neglected to simplify the analysis. The assumption is applicable to the KUCA system. Consequently, the discrete form of Eq. (2.51) on time domain is described as

$$N(t_j) = \frac{\Lambda}{\beta - \rho} Q(t_j) + \frac{\Lambda S}{\beta - \rho}, \quad (2.53)$$

$$Q(t_j) = \sum_{k=1}^6 \lambda_k C_k(t_j), \quad (2.54)$$

where  $t_j$  is the  $j$ th discrete time. As the time-dependent neutron density  $N(t_j)$ , the time-sequence count data were employed. The time-dependent precursor density  $C_k(t_j)$  of delayed neutrons can be obtained by solving numerically Eq. (2.52). In this study, the implicit time-integration method was employed to obtain the precursor density. When the time-sequence data  $N(t_j)$  and  $Q(t_j)$  are plotted on the  $x$ - $y$  coordinate, two unknown constants, i.e., the reactivity and the source strength, can be determined from the least-squares fitting of Eq. (2.53) to these data. By applying the LSIKM to beam trip data, Eq. (2.53) is reduced to

$$N(t_j) = \frac{\Lambda}{\beta - \rho} Q(t_j), \quad (2.55)$$

where the source strength is set to zero.

The delayed neutron data and prompt-neutron generation time of the present reactor system were generated using the SRAC code system [34], where a three-dimensional, 19-energy-group diffusion calculation was done with JENDL-3.2 nuclear library [35].

### 2.3.2.2 Integral Count Technique

The integral count technique has been frequently employed to determine the subcriticality from a source jerk experiment and a rod drop one [31, 36]. When a neutron source is rapidly taken out of a subcritical reactor core or a control rod is dropped into a critical core at  $t = 0$ , the reactivity of the core can be expressed as

$$\rho = - \sum_{k=1}^6 \frac{\beta_k}{\lambda_k} \frac{N(0)}{\int_0^{\infty} N(t) dt}. \quad (2.56)$$

The above expression is a familiar formula for the integral count technique.

The technique is also applied to the present beam trip experiment. Prior to beam trip operation, the average count rate used as  $N(0)$  is measured using a conventional counting scaler. Then, the integral counts after the operation, which can be used as an integral appearing in the denominator of Eq. (2.56), are also measured using the scaler.

### 2.3.3 Results and Discussion

#### 2.3.3.1 Time-Sequence Data

Figure 2.22 shows the time-sequence  $N(t)$  and  $Q(t)$  data obtained from counter B4 in a beam trip experiment, where the control rod pattern is A and the beam is turned off at zero time. The time-sequence  $N(t)$  data in this figure are indicated as instantaneous count rate at every 0.1 s. After the beam trip,  $N(t)$  and  $Q(t)$  promptly decrease and then asymptotically tend to zero. The statistical fluctuation of  $Q(t)$  defined using Eq. (2.54) is slight, compared with that of  $N(t)$ . This is because the delayed-neutron emission rate  $Q(t)$  is an integral quantity of  $N(t)$  over a passing time. The least-squares approximation fits a model function with minimum error on the y-axis assuming no error on the x-axis. Therefore, the time-sequence  $Q(t)$  and  $N(t)$  data should be assigned to x- and y-axis variables, respectively, for successful least-squares fitting on the x-y coordinate.

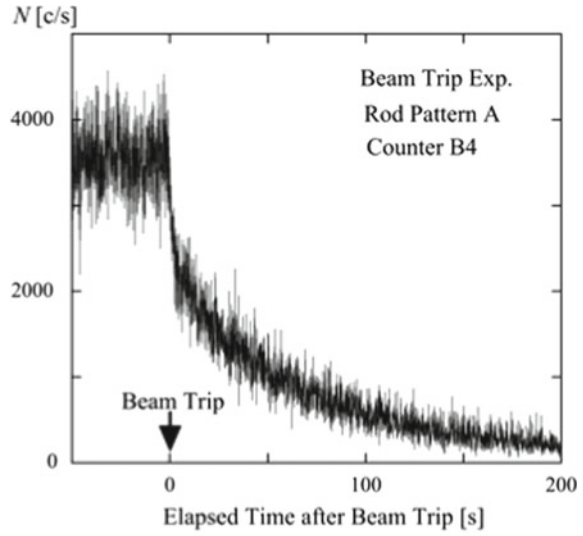
Figure 2.23 shows the time-sequence  $N(t)$  and  $Q(t)$  data obtained from counter B4 in a beam restart experiment, where the control rod pattern is A and the beam is turned on at zero time. After the beam restart,  $N(t)$  and  $Q(t)$  promptly increase and then asymptotically tend to their individual constants.

#### 2.3.3.2 Least-Squares Fitting

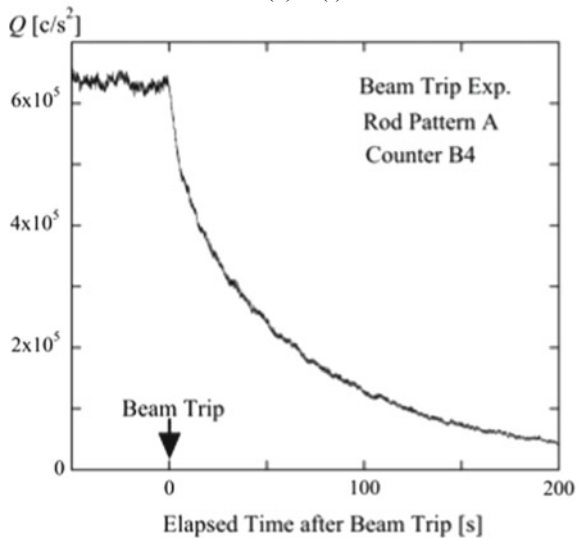
In Fig. 2.24, the above  $Q(t)$  and  $N(t)$  data are plotted on the x-y coordinate, where the fitted lines are drawn by a straight line. Equations (2.55) and (2.53) were fitted to the data sets of Fig. 2.24a, b, respectively. The fitting is successful and the subcritical reactivity can be determined from the slope of the fitted line.

Table 2.3 summarizes the reactivities obtained from the beam trip and restart experiments. As the errors of these results of the LSIKM, the statistical uncertainties that originated from the least-squares fit were employed, while the uncertainty of delayed-neutron yield  $\beta$  was not taken into account. The errors of the integral count technique were estimated from counting statistics. For comparison, the results obtained by a pulsed neutron experiment [11] are also shown in Table 2.4, where the subcriticality obtained by a conventional analysis technique has a significant counter-position dependence. This dependence is originated from a higher mode excited by

**Fig. 2.22** Time-sequence data  $N(t)$  and  $Q(t)$  in a beam trip experiment (Ref. [28])



(a)  $N(t)$

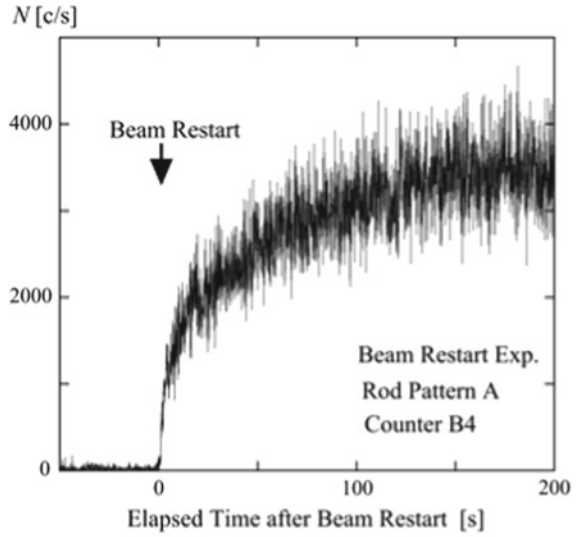


(b)  $Q(t)$

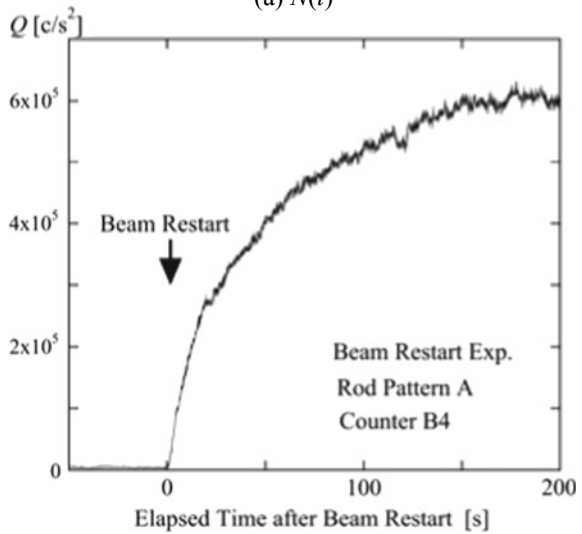
a pulsed neutron source. The mask analysis technique was employed to reduce the dependence.

It is obvious from Table 2.3 that counter B1 significantly overestimates the subcriticality. This feature is originated from a large amount of source neutrons traveling from the DT target. This is because the counter relatively close to the target counts much more the source neutrons during successive pulse injection, and then the source neutrons decay out with a larger decay constant after beam trip and more steeply

**Fig. 2.23** Time-sequence data  $N(t)$  and  $Q(t)$  in a beam restart experiment (Ref. [28])



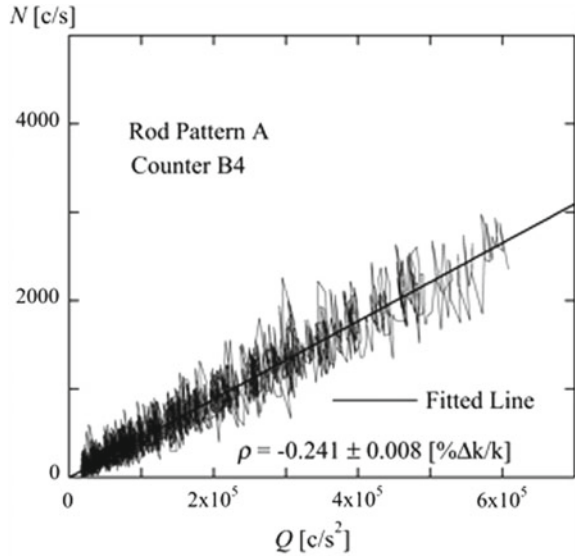
(a)  $N(t)$



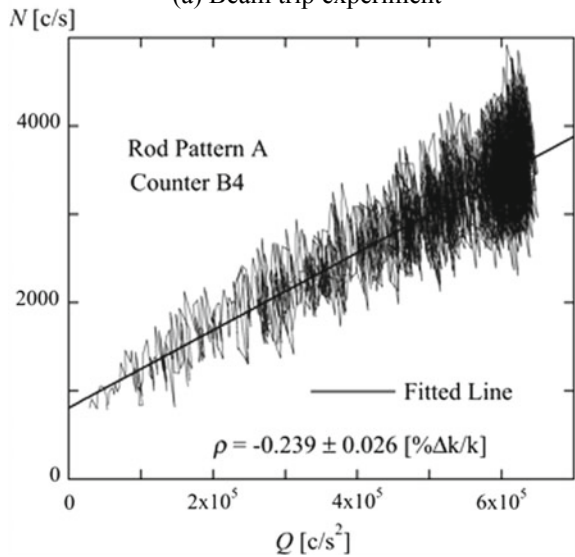
(b)  $Q(t)$

increase after beam restart. The decay of fission neutrons contains information on the reactivity, while that of the source neutrons is free from such information. Generally, the decay constant of the source-neutron mode free from the neutron-production process is larger than that of the prompt mode of the fission neutron [11]. In Fig. 2.25, the decay data of counter B1 are compared with those of B4 in a beam trip experiment, where the control rod pattern is C and the data is normalized in such a way that the average counts before the beam trip become one. This figure shows a larger

**Fig. 2.24** Plot of variables and fitted line on  $x$ - $y$  coordinate (Ref. [28])



(a) Beam trip experiment



(b) Beam restart experiment

decay of B1 data just after the trip, as noted above. For an actual ADS, a neutron counter should be placed at a position far from a spallation target. Table 2.3 also shows that the results of the LSIKM for beam trip data are consistent with those of the integral count technique except for counter B1.

As seen from Tables 2.3 and 2.4, the present subcriticality obtained using the counters other than B1 has a slight counter-position dependence compared with



**Table 2.3** Reactivity obtained by beam trip and restart experiments [% $\Delta k/k$ ] (Ref. [28])

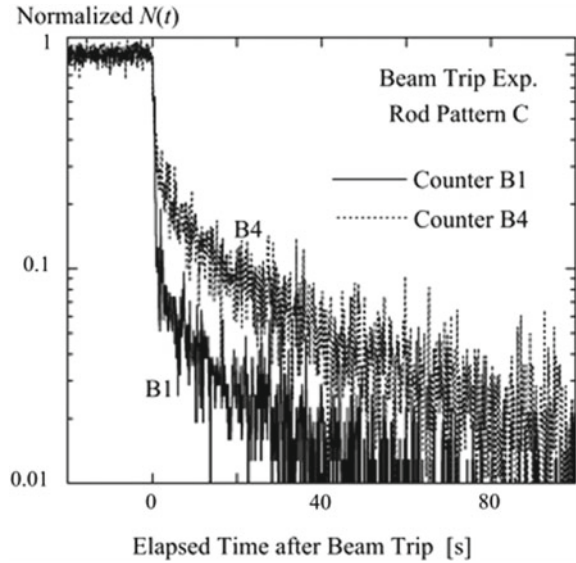
Rod	Neutron	Beam trip experiment		Beam restart
Pattern	Counter	LSIKM	Integral	Experiment <sup>a</sup>
A	B1	$-0.283 \pm 0.010$	$-0.288 \pm 0.020$	$-0.340 \pm 0.034$
	B2	$-0.244 \pm 0.008$	$-0.232 \pm 0.012$	$-0.242 \pm 0.025$
	B3	$-0.244 \pm 0.009$	$-0.233 \pm 0.016$	$-0.241 \pm 0.028$
	B4	$-0.241 \pm 0.008$	$-0.232 \pm 0.012$	$-0.239 \pm 0.026$
B	B1	$-1.293 \pm 0.018$	$-1.115 \pm 0.054$	$-1.278 \pm 0.083$
	B2	$-0.641 \pm 0.008$	$-0.617 \pm 0.026$	$-0.632 \pm 0.035$
	B3	$-0.631 \pm 0.009$	$-0.612 \pm 0.034$	$-0.625 \pm 0.042$
	B4	$-0.617 \pm 0.008$	$-0.599 \pm 0.026$	$-0.593 \pm 0.033$
C	B1	$-5.082 \pm 0.094$	$-4.065 \pm 0.256$	$-2.698 \pm 0.423$
	B2	$-1.599 \pm 0.025$	$-1.513 \pm 0.092$	$-1.460 \pm 0.165$
	B3	$-1.555 \pm 0.033$	$-1.501 \pm 0.120$	$-1.447 \pm 0.201$
	B4	$-1.504 \pm 0.027$	$-1.431 \pm 0.084$	$-1.355 \pm 0.171$

<sup>a</sup>LSIKM applied**Table 2.4** Reactivity obtained by pulsed neutron experiments [% $\Delta k/k$ ] (Ref. [28])

Rod	Neutron	Pulsed neutron experiment	
Pattern	Counter	Conventional	Mask technique
A	B1	$-16.05 \pm 0.68$	$-0.236 \pm 0.039$
	B2	$-0.299 \pm 0.042$	$-0.223 \pm 0.038$
	B3	$-0.153 \pm 0.036$	$-0.227 \pm 0.039$
	B4	$-0.043 \pm 0.036$	$-0.245 \pm 0.039$
B	B1	$-16.25 \pm 0.69$	$-0.644 \pm 0.055$
	B2	$-0.872 \pm 0.065$	$-0.642 \pm 0.054$
	B3	$-0.622 \pm 0.053$	$-0.658 \pm 0.055$
	B4	$-0.359 \pm 0.049$	$-0.668 \pm 0.055$
C	B1	$-18.09 \pm 0.73$	$-1.616 \pm 0.092$
	B2	$-2.342 \pm 0.126$	$-1.554 \pm 0.089$
	B3	$-1.497 \pm 0.087$	$-1.572 \pm 0.090$
	B4	$-0.952 \pm 0.075$	$-1.565 \pm 0.089$

those obtained in a conventional pulsed neutron experiment and agrees with the result of the pulsed neutron experiment based on the mask analysis within experimental errors. Here, we note a further observation from this table, which is a larger error of the beam restart experiment than that of the beam trip one. From the least-squares fitting of Eq. (2.55) to beam trip data, only the reactivity is determined. From the fitting of Eq. (2.53) to beam restart data, however, not only is the reactivity but also the source strength is simultaneously determined. The additional unknown constant

**Fig. 2.25** Difference in decay data between counters B1 and B4 (Ref. [28])



to be inferred is responsible for the larger error of the beam restart experiment. For the smaller error, the trip experiment is advantageous. Nevertheless, the restart experiment is useful for the simultaneous determination of both the reactivity and source strength.

## 2.4 Conclusion

We derived the Feynman- $\alpha$  and the Rossi- $\alpha$  formulae applicable to the respective correlation data analyses for a pulsed non-Poisson neutron source. These formulae were applied to the Feynman- $\alpha$  and the Rossi- $\alpha$  analyses for a subcritical system driven by a pulsed spallation source in KUCA. The prompt-neutron decay constant determined from the present Feynman- $\alpha$  analysis well agreed with that done from a previous analysis for the same subcritical system driven by an inherent neutron source. However, the decay constant determined from the present Rossi- $\alpha$  analysis was in poor agreement with that done from the above previous analysis. When the data around the convex top were masked for least-squares fitting of the present Rossi- $\alpha$  formula, the disagreement could be successfully resolved. When the respective prompt-neutron correlation amplitudes determined from the present Feynman- $\alpha$  and Rossi- $\alpha$  analyses were compared with those done from the previous analyses under the Poisson inherent source, the non-Poisson spallation source definitely enhanced the respective correlation amplitudes.

The Degweker's factor  $(m_2 - m_1^2)/m_1^2$  of  $0.067 \pm 0.011$ , which is a quantitative indication of the non-Poisson character, could be determined from the present Rossi- $\alpha$  analysis.

The power spectral analysis on frequency domain was conducted in the same A-core as the above Feynman- $\alpha$  and Rossi- $\alpha$  analyses. Not only the cross-power but also the auto-power spectral density had a considerable correlated noise component even at a deeply subcritical state, where no correlated component could be observed under a pulsed DT(14 MeV) neutron source. The non-Poisson character of the spallation source must enhance the correlation amplitude of these power spectral densities. The Degweker's factor of  $0.082 \pm 0.021$  could be determined from the present analysis and was consistent with that obtained by the above Rossi- $\alpha$  analysis.

An experimental technique based on accelerator-beam trip and restart operation was proposed to determine the subcritical reactivity of ADS. A series of these experiments was performed in a subcritical thermal core of KUCA. The results demonstrated the applicability of the proposed technique to the thermal ADS of KUCA. We expect the proposed technique to be applied for an actual ADS in start-up or shut-down operation.

## References

1. Nakajima K, Sano T, Hohara S et al (2021) Feynman- $\alpha$  and Rossi- $\alpha$  analyses for a subcritical reactor system driven by a pulsed spallation neutron source in Kyoto University Critical Assembly. *J Nucl Sci Technol* 58:117
2. Nakajima K, Sano T, Takahashi et al (2020) Source multiplication measurements and neutron correlation analyses for a highly enriched uranium subcritical core driven by an inherent source in Kyoto University Critical Assembly. *J Nucl Sci Technol* 57:1152
3. Nagaya Y, Okumura K, Sakurai T et al (2016) MVP/GMVP Version3: general purpose Monte Carlo codes for neutron and photon transport calculations based on continuous energy and multigroup methods. JAEA-Data/Code 2016-018
4. Nagaya Y, Okumura K, Mori T (2015) Recent developments of JAEA's Monte Carlo code MVP for reactor physics applications. *Ann Nucl Energy* 82:85
5. Shibata K, Iwamoto O, Nakagawa T et al (2011) JENDL-4.0: a new library for nuclear science and technology. *J Nucl Sci Technol* 48:1
6. Rana YS, Degweker SB (2009) Feynman-alpha and Rossi-alpha formulas with delayed neutrons for subcritical reactors driven by pulsed non-poisson sources. *Nucl Sci Eng* 162:117
7. Williams MMR (1974) *Random processes in nuclear reactors*. Pergamon Press, Oxford, UK, pp 26–49
8. Degweker SB, Rana YS (2007) Reactor noise in accelerator driven systems-II. *Ann Nucl Energy* 34:463
9. Okuda R, Sakon A, Hohara S et al (2016) An improved Feynman- $\alpha$  analysis with a moving-bunching technique. *J Nucl Sci Technol* 53:1647
10. Tonoike K, Miyoshi Y, Kikuchi T et al (2002) Kinetic parameter  $\beta_{\text{eff}}/\ell$  measurement on low enriched uranyl nitrate solution with single unit cores (600 $\phi$ , 280T, 800 $\phi$ ) of STACY. *J Nucl Sci Technol* 39:1227
11. Taninaka H, Hashimoto K, Pyeon CH et al (2010) Determination of lambda-mode eigenvalue separation of a thermal accelerator-driven system from pulsed neutron experiment. *J Nucl Sci Technol* 47:376

12. Sakon A, Hashimoto K, Maarof MA et al (2014) Measurement of large negative reactivity of an accelerator-driven system in the Kyoto University Critical Assembly. *J Nucl Sci Technol* 51:116
13. Furuhashi A (1962) Characteristic spectra in neutron thermalization. *J At Energy Soc Jpn* 4:677
14. Takahashi H (1962) Space and time dependent eigenvalue problem in neutron thermalization. EURATOM, EUR-22.e
15. Pazsit I, Yamane Y (1998) Theory of neutron fluctuations in source-driven subcritical systems. *Nucl Instrum Methods A* 403:431
16. Pazsit I, Yamane Y (1998) The variance-to-mean ratio in subcritical systems driven by a spallation source. *Ann Nucl Energy* 25:667
17. Behringer K, Wydler P (1999) On the problem of monitoring the neutron parameters of the fast energy amplifier. *Ann Nucl Energy* 26:1131
18. Kuang ZF, Pazsit I (2000) A quantitative analysis of the Feynman- and Rossi-alpha formulas with multiple emission sources. *Nucl Sci Eng* 136:305
19. Diven BC, Martin HC, Taschek RF et al (1956) Multiplicities of fission neutrons. *Phys Rev* 101:1012
20. Letourneau A, Galin J, Goldenbaum F et al (2000) Neutron production in bombardments of thin and thick W, Hg, Pb targets by 0.4, 0.8, 1.2, 1.8 and 2.5 GeV protons. *Nucl Instrum Methods Phys Res B* 170:299
21. Nakajima K, Sakon A, Sano T et al (2021) Power spectral analysis for a subcritical reactor system driven by a pulsed spallation neutron source in Kyoto University Critical Assembly. *J Nucl Sci Technol* 58:374
22. Keepin GR, Wimett TF, Zeigler RK (1957) Delayed neutrons from fissionable isotopes of Uranium Plutonium and Thorium. *Phys Rev* 107:1044
23. Sakon A, Hashimoto K, Sugiyama W et al (2013) Power spectral analysis for a thermal subcritical reactor system driven by a pulsed 14 MeV neutron source. *J Nucl Sci Technol* 50:481
24. Nomura T (1965) Improvement in S/N ratio of reactor noise spectral density. *J Nucl Sci Technol* 2:76
25. Akcasu AZ, Osborn RK (1966) Application of Langevin's technique to space- and energy-dependent noise analysis. *Nucl Sci Eng* 26:13
26. Sheff JR, Albrecht RW (1966) The space dependence of reactor noise I—theory. *Nucl Sci Eng* 24:246
27. Hashimoto K, Nishina K, Tatematsu A et al (1991) Theoretical analysis of two-detector coherence functions in large fast reactor assemblies. *J Nucl Sci Technol* 28:1019
28. Taninaka H, Hashimoto K, Pyeon CH et al (2011) Determination of subcritical reactivity of a thermal accelerator-driven system from beam trip and restart experiment. *J Nucl Sci Technol* 48:873
29. Pyeon CH, Hervault M, Misawa T (2008) Static and kinetic experiments on accelerator-driven system with 14 MeV neutrons in Kyoto University Critical Assembly. *J Nucl Sci Technol* 45:1171
30. Hashimoto K, Ohya K, Yamane Y (1996) Experimental investigation of dead-time effect on Feynman-  $\alpha$  method. *Ann Nucl Energy* 23:1099
31. Taninaka H, Hashimoto K, Ohsawa T (2010) An extended rod drop method applicable to subcritical reactor system driven by neutron source. *J Nucl Sci Technol* 47:351
32. Hoogenboom JE, van der Sluijs AR (1988) Neutron source strength determination for on-line reactivity measurements. *Ann Nucl Energy* 15:553
33. Tamura S (2003) Signal fluctuation and neutron source in inverse kinetics method for reactivity measurement in the sub-critical domain. *J Nucl Sci Technol* 40:153
34. Okumura K, Kaneko K, Tsuchihashi K (1996) SRAC95; general purpose neutronics code system. JAERI-Data/Code 96-015
35. Nakagawa T, Shibata K, Chiba S et al (1995) Japanese evaluated nuclear data library version 3 revision-2 JENDL-3.2. *J Nucl Sci Technol* 32:1259
36. Hogan WS (1960) Negative-reactivity measurements. *Nucl Sci Eng* 84:518

**Open Access** This chapter is licensed under the terms of the Creative Commons Attribution 4.0 International License (<http://creativecommons.org/licenses/by/4.0/>), which permits use, sharing, adaptation, distribution and reproduction in any medium or format, as long as you give appropriate credit to the original author(s) and the source, provide a link to the Creative Commons license and indicate if changes were made.

The images or other third party material in this chapter are included in the chapter's Creative Commons license, unless indicated otherwise in a credit line to the material. If material is not included in the chapter's Creative Commons license and your intended use is not permitted by statutory regulation or exceeds the permitted use, you will need to obtain permission directly from the copyright holder.

